to appear 1997 IEEE International Conference on Robotics and Automation

Some Basic Issues in Teletaction *

R.S. Fearing, G. Moy and E. Tan
Department of EE&CS
University of California
Berkeley, CA 94720-1770

Abstract

Teletaction is the transmission of cutaneous information from a remote tactile sensor to an operator's skin, typically the finger tips. Ideally, one would like a realistic sensation of directly touching an object with one's own finger and sense properties such as local shape, hardness, or texture. Teletaction or tactile feedback is one component of haptic feedback, the other component being force or kinesthetic feedback. This paper considers design issues for teletaction systems, particularly sampling density, aliasing, and the limitations of using an array of 1 DOF actuators to approximate a continuous stress distribution on the human finger.

1 Introduction

Most force-reflecting teleoperators do not provide information about texture, local compliance, or local shape. This information is important in applications such as surgery, where the feel of the environment provides knowledge that can not be obtained by purely visual means. One promising use for a teletaction system is in minimally invasive surgery. Fig. 1 suggests using a tactile sensor mounted on a catheter to allow a vascular surgeon to feel plaques, branches, or soft spots inside blood vessels. The teletaction system uses a tactile stimulator to create a pattern of stress on a finger tip. This pattern is ideally indistinguishable from direct contact of the finger with the environment. We discuss teletaction systems with high spatial detail but negligible dynamics. This information maps to the slowly adapting (SA) mechanoreceptors in the fingertip [Loomis and Lederman 1986].

First we overview the components of teletaction systems. Next we present a planar linear-elastic model for approximate system analysis. Using this model, we consider an idealized teletaction system. This idealization bounds real teletaction system performance for a particular sampling density. One fundamental limitation of teletaction systems is aliasing due to undersampling. Using psychophysical experiments, we obtain preliminary bounds on human fingertip sensitivity to errors due to aliasing.

*This work was funded in part by: NSF-PYI grant IRI-9157051 and NSF grant IRI-9531837.

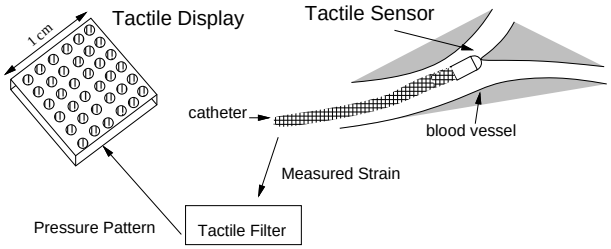

Figure 1: Example teletaction system.

Most teletaction work has focused on tactile sensors and stimulators [Shimoga 1992; Howe et al 1995]. Tactile sensors are comparatively well understood, (Howe [1994]) although generally designed for shape recognition and manipulation tasks, not teletaction. Typical tactile sensors range in size from 1 mm square with 8×8 elements [Gray and Fearing, 1996] to 16 mm square with 8×8 elements [Howe et al 1995] to a 25 mm diameter cylinder with 3×16 elements [Nicolson and Fearing 1995]. These sensors typically respond only to the normal component of strain.

Tactile stimulators started with tactile reading aids for the blind using piezoelectric-driven pins and direct pneumatic actuation [Bliss 1969]. Progress in teletaction displays has been slow, due to the demanding mechanical requirements. An ideal stimulator requires $50Ncm^{-2}$ peak pressure, 4 mm stroke, and 25 Hz bandwidth; that is, a power density of $5Wcm^{-2}$, with $1mm^{-2}$ actuator density. This ideal is far from what has been achieved. Tactile display designs have used solenoids [Fischer et al, 1995], shape memory alloy [Howe et al 1995; Hasser and Daniels 1996], and pneumatics [Cohn et al 1992]. Electrocutaneous stimulation [Kaczmarek et al 1991] is mechanically quite simple; however, the perceptual effects are hard to analyze.

After tactile sensors and tactile displays, the third key to teletaction system design is understanding human tactile sensing sensitivity, sensor density, and spatial and temporal frequency response [Loomis and Lederman 1986; Lamotte and Srinivasan 1993; Phillips and Johnson 1981]. Human tactile perception is not yet understood at the level of human visual perception that enabled practical color television systems. Signal-to-noise ratio and dynamic touch response at

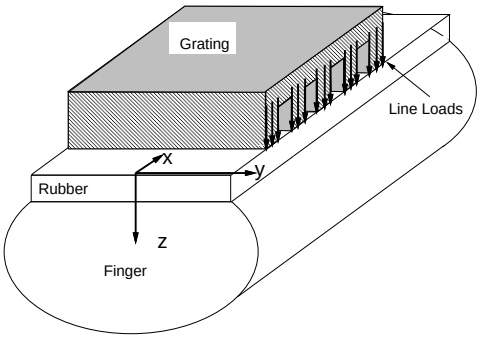

Figure 2: Finger geometry for plane stress assumption.

low temporal frequencies need to be determined. Better mechanistic models of touch receptors [Pawluk and Howe, 1996] will help.

2 Planar Linear Elastic Model

A compliant tactile sensor provides contact information from objects in the environment. For simplicity, we use the plane-stress approximation (Fig. 2). Consider a slice of elastic material in the $x-z$ plane with the applied force on top constant in the y direction, and the normal stresses on the face of the slice (σ_y) equal to 0. (See [Fearing 1990] for explanation of assumptions).

The stresses in the slice for a line load applied normal to the surface are [Johnson, 1985]:

$$\sigma_x = \frac{-2F_z z x^2}{\pi r^4} \ , \quad \sigma_z = \frac{-2F_z z^3}{\pi r^4} \ , \quad \tau_{xz} = \frac{-2F_z z^2 x}{\pi r^4} \ ,$$

where F_z is the force per unit thickness of the slice in Nm^{-1}, and $r^2 = x^2 + z^2$. For a concentrated tangential force F_x at the surface:

$$\sigma_x = \frac{-2F_x x^3}{\pi r^4} \ , \quad \sigma_z = \frac{-2F_x x z^2}{\pi r^4} \ , \quad \tau_{xz} = \frac{-2F_x z x^2}{\pi r^4} \ .$$

Since $\sigma_y = 0$ in the plane-stress approximation, the strains ϵ_x and ϵ_z will be a function of only σ_x and σ_z:

$$\epsilon_z \ = \ \frac{1}{E}[\sigma_z - \nu\sigma_x] \ \ , \quad \epsilon_x \ = \ \frac{1}{E}[\sigma_x - \nu\sigma_z] \ , \quad (1)$$

where E is the elastic modulus (Nm^{-2}), and ν is Poisson's ratio (typically $\nu \approx 0.5$ for rubber-like materials).

The normal strain ϵ_z has a component $h_z(x,\ z)$ due to F_z and a component $h_x(x,\ z)$ due to the tangential force component F_x . The *impulse response* for normal strain (with a unit line load applied at angle α) is defined as:

$$h(x,\ z) \ = \ h_z(x,\ z)\cos\alpha \ + \ h_x(x,\ z)\sin\alpha \ . \quad (2)$$

These simplified, planar models make reasonable predictions of the sensor behavior for various stimuli in some cases [Phillips and Johnson, 1981; Shimojo 1994; Fearing 1990]. See [Ellis and Qin 1994] for a finite element model.

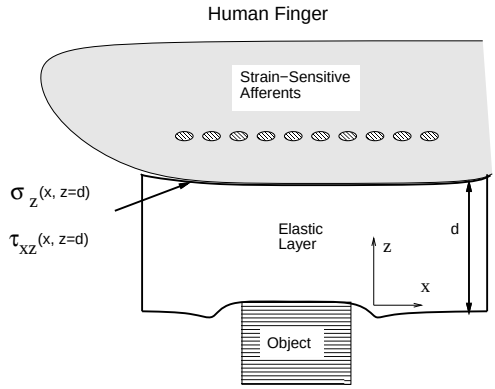

Figure 3: Example direct contact with rigid object through elastic layer.

3 Idealized Teletaction Mechanics

The teletaction system needs to provide the operator with the sensation that his or her own finger is touching the remote surface. The key problem is to find a set of forces which most closely approximates the actual contact. We define two types of teletaction systems: *Strain Matching* and *Stress Matching*. Consider a finger touching an object through an elastic layer which ideally has the same E and ν as the idealized finger. For ideal *Strain Matching*, we need a tactile display which generates identical strain in the finger mechanoreceptors as in the real contact. For ideal *Stress Matching*, we need a tactile display which generates identical stresses (to within the spatial sampling limit) on the finger surface.

Why is the elastic layer needed in the teletaction system? Consider the spatial impulse response of the teletaction system, i.e. the response to a pin prick. If the tactile sensor does not have a spatial low-pass filter, it is impossible to localize the pin to better than one tactel, no matter how dense the sensors, and the pin may be between sensors and not sensed. Since it is very difficult to achieve stimulator density comparable to human mechanoreceptor density (on the order of $200cm^{-2}$), an elastic layer, which acts as a spatial low-pass filter, is essential. Otherwise, the user would feel an array of pins instead of a smooth contact. If high-density high-stress actuators were available for a display, a low-pass filter would then be necessary to prevent skin damage when touching sharp objects. Thus, the best teletaction system feels like touching the real world through an elastic layer, or glove. The higher the sensor and stimulator density, the thinner the glove can be without introducing spatial sampling artifacts.

3.1 Teletaction: Stress Matching

Consider the real contact of Fig. 3 replaced with a tactile stimulator such that the normal and shear stresses on the finger $\sigma_z(x, z = d)$, $\tau_{xz}(x, z = d)$ are the same to within the noise sensitivity of the finger. Fig. 4 shows how this could be done. Ideally,

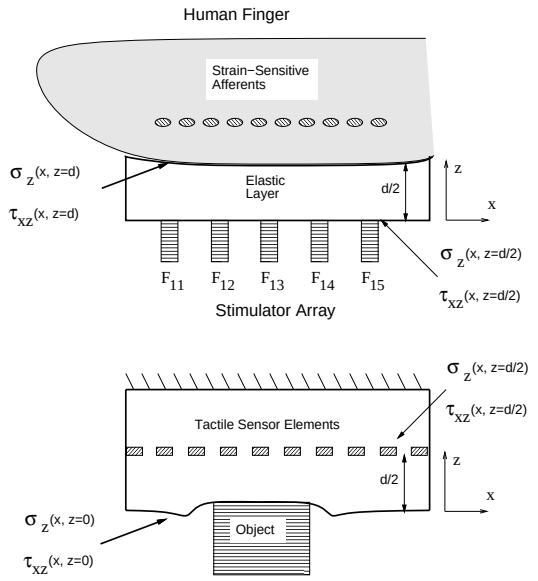

Figure 4: Tactile sensor and tactile stimulator principles for stress matching.

the normal and shear stresses on the boundary $z = \frac{d}{2}$ are continuously sensed and exactly replicated on the elastic layer covering the finger. Since the boundary conditions match at the top of the finger layer and the bottom of the tactile sensor layer, the two layers act as one layer of thickness d. Thus the finger would sense exactly what was sensed in Fig. 3.

In practice, most tactile sensors measure the normal component of the strain (ϵ_z) at depth $\frac{d}{2}$, not both components of stress. An exception is [Domenici and DeRossi 1992]. Also, the measurements are spatially sampled, not continuous, so information is lost due to aliasing. Further, current stimulators apply only normal forces not tangential. The problem is to choose the stimulator forces, F_{ij}, so that the stress on the human finger is as close as possible to the the real contact stress.

3.2 Teletaction: Strain Matching

Instead of matching surface stresses, we can match strains. This could be an easier problem, as the cutaneous mechanoreceptors may respond best to only one component of strain; i.e. they are scalar rather than tensor sensor elements. Phillips and Johnson [1981] suggest that an individual SA mechanoreceptor's response correlates best with the maximum compressive strain, independent of direction. For this paper, we assume normal strain ϵ_z and frictionless indentation for simplicity. Determination of stresses and strains of a real contact would be complicated without giving more insight to the basic problem.

Using a linear, space-invariant model for the elastic medium, for surface normal load $p(x)$, the normal strain at depth d is $\epsilon_z(x, z = d) = h_z(x, d) * p(x)$.

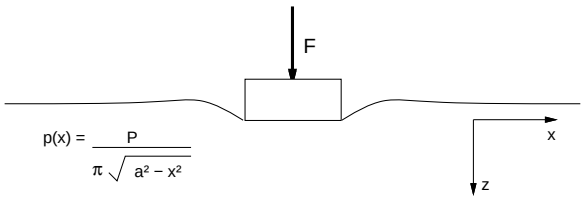

Figure 5: Example pressure distribution for rectangular indentor with frictionless indentation.

Discretizing the problem,

$$\epsilon_s = E_s p \quad (3)$$
$$\epsilon_f = E_f S f \quad (4)$$

where ϵ_f is the strain in the human finger, ϵ_s is measured strain in the tactile sensor, E_s and E_f are the maps from surface pressure to measured strain in the sensor and finger respectively, p is the pressure on the sensor, f is the discrete set of stimulator points applying normal forces to the finger, and S is a sampling matrix. (The sampling matrix inserts zero force elements to match the size of the map matrix E_f). For the ideal strain matching method, we want $\epsilon_f = \epsilon_s$.

Using a least-squares approach, in principle the optimal force vector can be found from

$$f = [(E_f S)^T (E_f S)]^{-1} (E_f S)^T \epsilon_s. \quad (5)$$

As high sensing density is easier to achieve than high stimulator density, we assume that $\epsilon_s(x)$ can be accurately recovered by interpolation. We note several difficulties with this approach, such as changes in position and temporal scales, hysteresis, non-linearities, and that the human finger likely measures maximum compressive strain, not normal strain. Although low-pass filtering the tactile sensor makes the inverse map poorly conditioned, it also lowers required stimulator spatial resolution. Note that while f may be poorly reconstructed, it will be low-pass filtered by $E_f S$.

Let's consider a numerical example showing strain matching for a rectangular indentor (Fig. 5). We assume a stimulator spacing of 1 mm, sensor depth of 1.5 mm, and rectangular indentor width of 4 mm. (For calculation, pressure and strain are discretized at 0.1 mm spacing). For numerical purposes, Fig. 6 shows the good matching between normal strain in tactile sensor ϵ_s and the resulting strain in the finger ϵ_f. Note that the stimulator values have not been regularized, hence the noisy appearance. Approaches described in [Nicolson and Fearing 1993] or [Ellis and Qin 1994] could regularize the tactor forces and ensure that they are all compressive. The elastic layer between the display pins and finger has in effect regularized the surface stress, and the sensed strain in the finger could be quite similar to the sensed strain in the tactile sensor.

3.3 Shape Based Teletaction

An alternative method for teletaction is to "... reproduce the object's contour so that it contacts the ap-

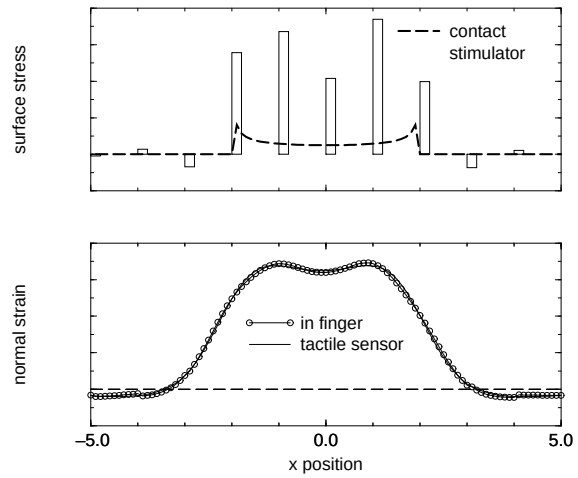

Figure 6: Equivalence of sampled surface stress profile and actual surface stress when measured by sub-surface strain sensors such as in the human finger. The top graph compares surface stress on the tactile sensor with the discrete surface stress which would be generated by a tactile display. The bottom graph compares the normal strain component in the tactile sensor and in a user's finger.

propriate part of the human hand" [Hagner and Webster 1989]. While the concept seems appealing, it has some limitations. First, as seen in Fig. 5, the surface deflection on the tactile sensor is not the same as the object shape – a shape and pressure from strain problem must be solved first to recover object shape and contact extent [Nicolson and Fearing, 1993]. In fact, a similar poorly conditioned map as in eq. (5) would be needed for shape display. The net loading on the finger would need to be controlled to insure that contact areas and stresses were consistent with the tactile sensor. Additionally, the shape display makes it difficult to present shear stresses or tensile forces, which may be possible with the strain matching approach. Finally, it is hard to build a stiff display which feels like a rigid object – the elastic layer is still needed for anti-aliasing.

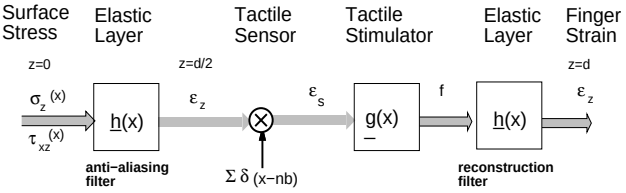

Figure 7: Signal flow model for a strain matching tactile sensor and stimulator combination.

4 Aliasing

Aliasing arises in the teletaction system from sampling by the tactile sensor and stimulator. In the signal flow model for *Strain Matching* (Fig. 7) (or *Stress Matching* (Fig. 8)), $\underline{h}(x)$ is the strain ($\underline{h}'(x)$ is the stress) response for an elastic layer of thickness $\frac{d}{2}$. The filter function $\underline{g}(x)$ converts discrete strain samples from the tactile sensor to a discrete set of forces F_{ij}, for example using eq. (5). With *Stress Matching*, we directly apply measured stress samples to the finger. Typically, the normal component of strain, ϵ_z, or the normal and shear components of stress, σ_z and τ_{xz}, will be sampled, and only normal components of force will be applied by the tactile stimulator. In signal processing terms, the elastic layers function as an anti-aliasing filter and a reconstruction filter. The amount of aliasing depends on the variable $\psi = \frac{b}{d/2}$, the ratio between sampling period, b, and the depth of a rubber layer, d/2.

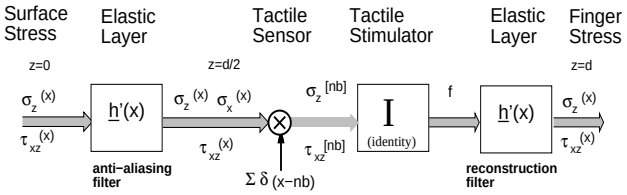

Figure 8: Signal flow model for a stress matching tactile sensor and stimulator combination.

4.1 Reconstruction with and without τ_{xz}

In addition to aliasing, reconstruction errors also arise since current tactile displays are incapable of controlling surface shear stress. Thus, it is necessary to model the system without transmission of the shear stress. In some applications, such as telesurgery, the objects being sensed are slippery and are close to being frictionless, which leads to no shear forces on the surface. However, zero shear stress on the surface does not imply zero shear stress at depth $\frac{d}{2}$.

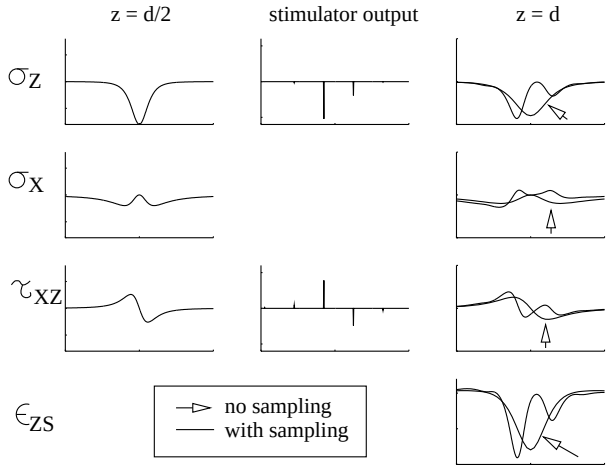

Figure 9: The stresses, σ_z, σ_x, and τ_{xz} with $\psi = 2$.

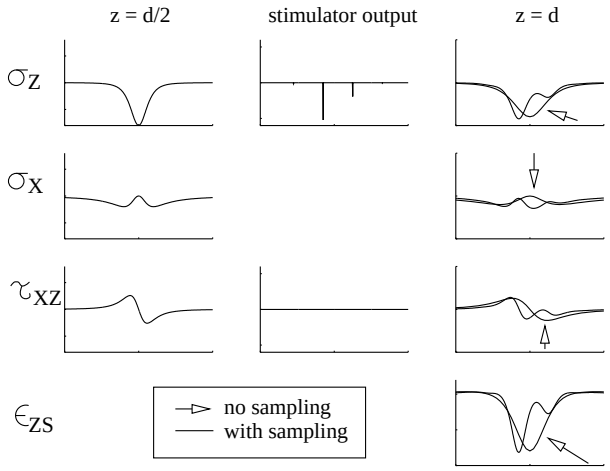

Figure 10: The stresses, σ_z, σ_x, and τ_{xz} with $\psi = 2$ and zeroing of τ_{xz} after sampling.

To see the effects with and without the transmission of shear stress τ_{xz} at depth $\frac{d}{2}$, a stress matching approach (Fig. 8) is used for the case of a normal line load contact.

To calculate the normal strain in the finger, we assume the stresses σ_z and τ_{xz} at depth $\frac{d}{2}$, are sampled with period b. The sampled stresses are passed through the reconstruction filter resulting in the finger stresses, σ_z and τ_{xz}, at depth d. Using σ_z and σ_x at depth d, ϵ_{zs} is calculated with eq. (1). Figure 9 shows sampling of the intermediate stresses used to calculate the normal strain. Figure 10 shows the same information, except that the shear stress is zeroed out after sampling. In both of these simulations, the spatial sampling occurred a quarter period out of phase with respect to the point of the load.

4.2 Aliasing Error Metric

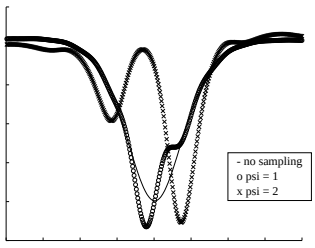

Figure 11: Normal strain in the finger ϵ_z due to a normal line load with no sampling, $\psi = 1$ and $\psi = 2$.

To measure the error in ϵ_z due to aliasing, we define the signal-to-noise ratio to be:

$$SNR = 10log_{10}\left(\frac{\int_{-\infty}^{\infty}\epsilon_z^2(x)dx}{\int_{-\infty}^{\infty}[\epsilon_z(x)-\epsilon_{zs}(x)]^2dx}\right)$$

Contact type	SNR
line load (normal)	16
line load (30°)	11
block indentor with width 20 (normal)	19
block indentor with width 20 (30°)	7
cylindrical indentor width 20 (normal)	19
cylindrical indentor width 20 (30°)	8

Table 1: SNR with no shear stress transmission, no sampling, and d = 4.

where ϵ_{zs} is the strain in the z direction with sampling. In this definition, the signal is the reconstructed normal strain profile without sampling, and noise is the difference between the reconstructed normal strain profile with and without sampling. Figure 11 shows ϵ_z with no sampling, $\psi = 1$, and $\psi = 2$. Figure 12 shows the signal-to-noise ratio as a function of ψ. This model determines how thick the rubber layers should be for a given sampling period and signal-to-noise ratio. When sampling, the phase at which the samples are taken is very important. For the signal-to-noise ratio, the worst phase for each ψ was used. Even with no sampling, the SNR of the reconstructed normal strain without transmission of shear stress has an upper bound of 16 dB. Table 1 shows the effects of not transmitting shear stress at depth $\frac{d}{2}$ on the SNR using a variety of inputs and no sampling.

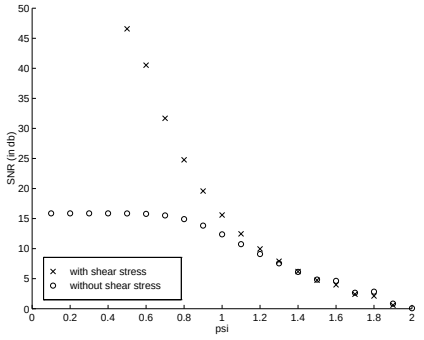

Figure 12: SNR vs. ψ with a normal line load input. If the stimulator can not display shear stress, the SNR is limited to 16 dB

Thus, shear stress information is important for high fidelity tactile stimulators. If a tactile stimulator has $\psi > 1$, then having shear stress information transmitted does not increase the SNR.

5 Human Sensitivity to Aliasing

The teletaction system should be designed so that the aliasing energy of the strain signal is undetectable. One way to test whether aliasing is detectable is to consider whether a sampled and low-pass filtered "DC" signal feels like a "DC" signal. We did a simple

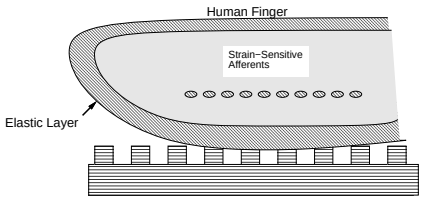

Figure 13: A human subject feels a grating through a 2 mm thick silicone rubber spatial low-pass filter layer.

psychophysics experiment as shown in Fig. 13 to quantify human sensitivity to aliasing. Consider touching a grating which has a spatial frequency much less than human mechanoreceptor density. The grating bars represent the spacing of a passive set of tactile stimulators. The grating attenuation by the elastic layer can be approximately predicted. If the residual strain signal is below the detectable threshold, then the filtered grating will feel the same as a smooth surface. Hence, aliasing will not be noticeable with this stimulator density and layer thickness.

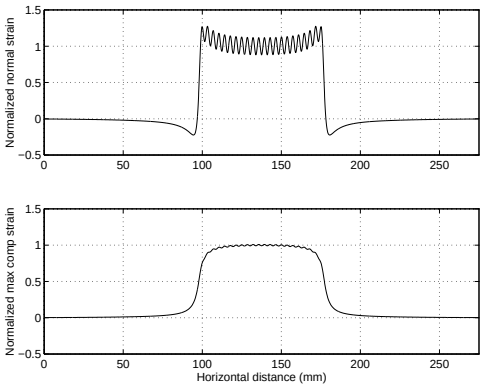

Figure 14: An example predicted sub-surface strain for a 3.6 mm grating period and sensors at a depth of 2.7 mm. The first graph shows what a tactile sensor responsive to normal strain would sense. The second graph shows the maximum compressive strain component, regardless of direction. Phillips and Johnson [1981] show that recordings from slowly adapting afferents agree most closely with the maximum compressive strain model.

Using the planar elastic model and the method of Phillips and Johnson [1981], we calculated surface stress and sub-surface strain for a range of 50% duty-cycle gratings, an example of which is shown in Fig. 14. The modulation index is defined as the peak-to-peak variation in strain divided by the average strain in the center of the contact region. Since we assume a logarithmic sensor response, the absolute level of force is not as important as the modulation index in detecting the grating. The grating period is greater than twice that which can be detected without a rubber layer, thus lack of detection is due to sensor noise, not lack of sufficient sensor sampling density. Fig. 15 shows the sharp drop-off in modulation index with increasing grating spatial frequency, for various sensor assumptions.

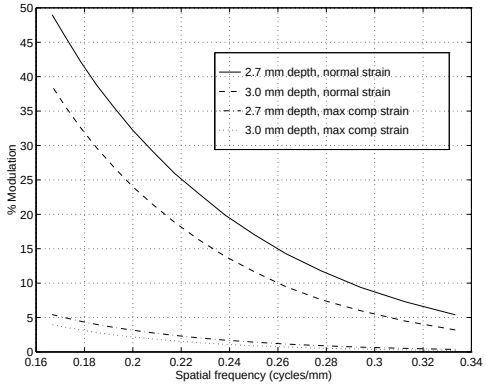

Figure 15: Modelled sub-surface modulation index for square grating patterns.

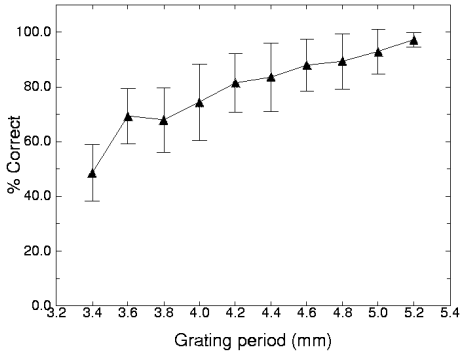

Figure 16: Average percentage correct for 7 subjects distinguishing between gratings and smooth blocks with a 2 mm glove.

5.1 Psychophysics Results

Experiments were performed on 7 subjects to determine their ability to distinguish various gratings from smooth blocks while wearing a custom molded 2 mm uniform glove on one finger. The experiment was of the forced choice type, where subjects were presented with a pair of contacts for 5 seconds, one smooth and one grating, and had to decide which was the grating. There were 10 different gratings; each grating was presented 20 times in random order. (For further details, see [Tan 1995]). The average for all trials and all subjects is shown in Fig. 16. No subjects were able to distinguish the 3.4 mm grating from smooth at above the chance level. Using a threshold of 75% correct, subjects varied from most sensitive, able to detect a 3.6 mm grating to least sensitive, with a 4.4 mm grating. Since we know the rubber thickness of 2.0 mm, and suppose mechanoreceptor depth of about

0.7 mm, we can predict the detectable modulation index for each subject. Unfortunately, we do not know exactly what mechanoreceptor strain sensing model is most appropriate for our contact situation. We can set some bounds for the most sensitive subject – a 3.6 mm grating corresponds to detectable modulation factors in the range of 2%, assuming a compressive strain sensor, to 10% assuming a shallow normal strain sensor. Thus, given a particular stimulator density, we can choose an elastic layer thickness to give a modulation index less than 10% or 2%.

6 Conclusions

We have presented some simplistic planar elastic models which can be used to help design teletaction systems. We have argued that teletaction is inherently limited to providing the sensation of touching the world through a glove, where high sampling density is needed to be able to use a relatively thin glove. As a rule of thumb, the elastic layer thickness should be greater than the stimulator spacing, and a ratio of spacing-to-thickness of 2:3 seems to work well using the strain matching technique. We have shown how using an elastic layer on a grating acts like a reconstruction filter which makes the surface perceptually smooth. Clearly, we need better mechanical models of finger skin and mechanoreceptors for more accurate predictions of human tactile sensing capabilities. With these better models, we can determine the specifications for teletaction systems, such as required force resolution, temporal bandwidth, sampling density, and elastic layer thickness. We can upper bound the human signal-to-noise ratio between 20 and 34 dB. From Fig. 12, we see that ψ must be less than 0.9 (with transmission of shear stress information) for aliasing to be below detectable levels for a normal line load input. Hence the stimulator pins will not be felt.

Acknowledgments

We thank John Lin for his work on the tactile stimulator, and K. Chiang, U. Singh and M. Fearing for helpful discussions and comments.

References

[1] J.C. Bliss, "A Relatively High-Resolution Reading Aid for the Blind", *IEEE Trans. on Man-Machine Sys.,* 10:1-9, 1969.

[2] M. Cohn, M. Lam, and R. Fearing. Tactile feedback for teleoperation. *SPIE Telemanip. Tech.*, 1833:240–254, 1992.

[3] P. Dario and M. Bergamasco, "An Advanced Robot System for Automated Diagnostic Tasks Through Palpation", *IEEE Trans. on Bio. Eng.*, 35(2): 118-126, Feb. 1988.

[4] C. Domenici, and D. DeRossi, "A Stress-component-selective tactile sensor array", *Sensors and Actuators* , vol. 13, pp. 97-100, 1992.

[5] R.E. Ellis and M. Qin, "Singular Value and Finite-Element Analysis of Tactile Shape Recognition" *IEEE Int. Conf. on Rob. and Auto.,* pp. 2529-2535, San Diego, CA, May 8-13, 1994

[6] R.S. Fearing. "Tactile sensing mechanisms." *Int. J. Rob. Res.*, 9(3):3–23, 1990.

[7] H. Fischer, B. Neisius, and R. Trapp, "Tactile Feedback for Endoscopic Surgery", *Interactive Technology and New Paradigm for Healthcare* , ed: K. Morgan, R.M. Satava, H.B. Sieburg, R. Mattheus, J.P. Christensen, pp. 114-117, IOS Press 1995.

[8] B. Gray and R.S. Fearing, " A surface-micromachined microtactile sensor array." *IEEE Int. Conf. Rob. and Auto.*, Minneapolis, April 1996.

[9] D.G. Hagner and J.G. Webster, "Telepresence for Touch and Proprioception in Teleoperator Systems", *IEEE Trans. on Systems, Man, and Cybernetics*, 18(6):1020-1023, Nov./Dec. 1988.

[10] C.J. Hasser and M.W. Daniels, "Tactile Feedback with Adaptive Controller for a Force-Reflecting Haptic Display", 15th Southern Biomedical Engineering Conf., pp. 526-533, Dayton, OH, 29-31 March 1996.

[11] R. Howe. "Tactile sensing and control of robotic manipulation." *Advanced Rob.*, 8(3):245–261, 1994.

[12] R.D. Howe, W.J. Peine, D.A. Kontarinis, and J.S. Son, "Remote Palpation Technology", *IEEE Eng. in Med. and Bio. Mag.* , pp. 318-323, May/June 1995.

[13] K.L. Johnson, *Contact Mechanics*, Cambridge University Press, 1985.

[14] K.A. Kaczmarek, J.G. Webster, P. Bach-y-Rita, and W.J. Tompkins, "Electrotactile and Vibrotactile Displays for Sensory Substitution Systems", *IEEE Trans. on Bio. Eng.* , 38(1): 1-16. Jan. 1991.

[15] R.H. Lamotte and M.A. Srinivasan, "Responses of cutaneous mechanoreceptors to the shape of objects applied to the primate fingerpad", *Acta Psychologica*, 84:41-51, 1993.

[16] J.M. Loomis and S.J. Lederman, "Tactual Perception", in *Handbook of Perception and Human Performance,* ed: K.R. Boff, L. Kaufman and J.P. Thomas, pp. 31-1:31-41, John Wiley and Sons: New York, 1986.

[17] E.J. Nicolson and R.S. Fearing, "Sensing Capabilities of Linear Elastic Cylindrical Fingers", *IEEE/RSJ Int. Conf. on Int. Rob. and Sys.*, Yokohama, Japan, July 1993.

[18] E.J. Nicolson and R.S. Fearing, "The Reliability of Curvature Estimates from Linear Elastic Tactile Sensors", *IEEE Int. Conf. on Rob. and Auto.*, Nagoya Japan, May 1995.

[19] D.T.V. Pawluk and R. D. Howe, "A Viscoelastic Model of the Human Fingerpad" Harvard Robotics Lab Tech. Rpt. 96-003.

[20] J.R. Phillips and K.O. Johnson, "Tactile Spatial Resolution III. A Continuum Mechanics Model of Skin Predicting Mechanoreceptor Responses to Bars, Edges, and Gratings," *J. of Neurophysiology* 46(6):1204-1225, 1981.

[21] K.B. Shimoga, "Finger Force and Touch Feedback Issues in Dextrous Telemanipulation", NASA-CIRSSE Int. Conf. on Intel. Rob. Sys. for Space Exploration, Troy, NY Sept. 30 - Oct 1, 1992.

[22] M. Shimojo, "Spatial Filtering Characteristic of Elastic Cover for Tactile Sensor", *IEEE Int. Conf. on Rob. and Auto.*, pp. 287-292, San Diego, CA, May 8-13, 1994

[23] E. Tan, "Estimating Human Tactile Resolution Limits for Stimulator Design", Master's Report, Dept of EECS, UC Berkeley, May 1995.